1521-009X/12/4009-1785–1796$25.00
DRUG METABOLISM AND DISPOSITION
Vol. 40, No. 9
46052/3789797

DMD 40:1785–1796, 2012

Preclinical Assessment of the Absorption and Disposition of the Phosphatidylinositol 3-Kinase/Mammalian Target of Rapamycin Inhibitor GDC-0980 and Prediction of Its Pharmacokinetics and Efficacy in Human

Laurent Salphati, Jodie Pang, Emile G. Plise, Leslie B. Lee, Alan G. Olivero, Wei Wei Prior, Deepak Sampath, Susan Wong, and Xiaolin Zhang

Departments of Drug Metabolism and Pharmacokinetics (L.S., J.P., E.G.P., S.W., X.Z.), Chemistry (A.G.O.), and Translational Oncology (L.B.L., W.W.P., D.S.) Genentech, Inc., South San Francisco, California

Received April 4, 2012; accepted June 13, 2012

ABSTRACT:

(*S*)-1-{4-[2-(2-Amino-pyrimidin-5-yl)-7-methyl-4-morpholin-4-yl-thieno[3,2-*d*]pyrimidin-6-ylmethyl]-piperazin-1-yl}-2-hydroxy-propan-1-one (GDC-0980) is a potent and selective inhibitor of phosphatidylinositol 3-kinase (PI3K) and mammalian target of rapamycin, two key components of the PI3K pathway, the deregulation of which is associated with the development of many cancers. The objectives of these studies were to characterize the absorption and disposition of GDC-0980 and assess its efficacy in an MCF7-neo/HER2 human breast cancer xenograft model in immunocompromised mice. Studies in parental Madin-Darby canine kidney cells indicated that GDC-0980 had high permeability (P_{app} = 18 × 10^{-6} cm/s), suggesting good absorption potential. However, it was found to be a P-glycoprotein and breast cancer resistance protein substrate in transfected cells and in knockout mice studies. Plasma protein binding was low, with the fraction unbound ranging from 29 to 52% across species. GDC-0980 hepatic clearance (CL) was predicted to be low in all of the species tested from hepatocyte incubations. The plasma CL of GDC-0980 was low in mouse (6.30 ml · min^{-1} · kg^{-1}), rat (15.4 ml · min^{-1} · kg^{-1}), and dog (6.37 ml · min^{-1} · kg^{-1}) and moderate in cynomolgus monkey (18.9 ml · min^{-1} · kg^{-1}). Oral bioavailability ranged from 14.4% in monkey to 125% in dog. Predicted human plasma CL and volume of distribution using allometry were 5.1 ml · min^{-1} · kg^{-1} and 1.8 l/kg, respectively. Parameters estimated from the pharmacokinetic/pharmacodynamic modeling of the MCF7-neo/HER2 xenograft data indicated that the GDC-0980 plasma concentration required for tumor stasis was approximately 0.5 μM. These parameters, combined with the predicted human pharmacokinetic profile, suggested that 55 mg once daily may be a clinically efficacious dose. GDC-0980 preclinical characterization and the predictions of its human properties supported its clinical development; it is currently in Phase II clinical trials.

Introduction

The phosphatidylinositol 3-kinase (PI3K)/Akt pathway plays a key role in cellular growth, survival, and differentiation (Engelman et al., 2006). Class I PI3Ks, with catalytic subunits α, β, γ, or δ, catalyze the phosphorylation of phosphatidylinositol 4,5-bisphosphate to phosphatidylinositol 3,4,5-trisphosphate. After this initial step, downstream kinases, among which are the serine/threonine protein kinases Akt and mammalian target of rapamycin (mTOR), in turn are activated. Aberrant regulation of this pathway has been implicated in several types of cancer, including breast, colon, and prostate (Engelman, 2009). Up-regulation of PI3K can occur through transforming mutations in the p110α subunit, loss of function of the phosphatase and tensin homolog, which counteracts the function of PI3K, or in response to receptor tyrosine kinase signaling (Chalhoub and Baker, 2009; Wong et al., 2010). Thus, this pathway has been identified as a promising target for the treatment of cancer, and numerous PI3K inhibitors have entered clinical trials (Ciraolo et al., 2011). In addition, inhibitors of the mTOR kinase, such as the rapamycin analogs (rapalogs) everolimus and temsirolimus, have shown activity in renal cell carcinoma and pancreatic tumors (Sabbah et al., 2011). However, mTOR functions as two protein complexes, mTORC1 and mTORC2, and the selectivity of rapalogs for mTORC1 does not prevent the phosphorylation and activation of Akt, possibly by mTORC2, through a feedback loop (O'Reilly et al., 2006; Guertin and Sabatini, 2009). Hence,

Article, publication date, and citation information can be found at http://dmd.aspetjournals.org.
http://dx.doi.org/10.1124/dmd.112.046052.

ABBREVIATIONS: PI3K, phophatidylinositol 3-kinase; A, apical; AUC_{inf}, area under the plasma concentration-time curve extrapolated to infinity; B, basolateral; BDC, bile duct-cannulated; BQL, below quantitation limit; CL, clearance; ER, efflux ratio; GDC-0941, 2-(1*H*-indazol-4-yl)-6-(4-methanesulfonyl-piperazin-1-ylmethyl)-4-morpholin-4-yl-thieno[3,2-*d*]pyrimidine; GDC-0980, (*S*)-1-{4-[2-(2-amino-pyrimidin-5-yl)-7-methyl-4-morpholin-4-yl-thieno[3,2-*d*]pyrimidin-6-ylmethyl]-piperazin-1-yl}-2-hydroxy-propan-1-one; GF120918, *N*-(4-[2-(1,2,3,4-tetrahydro-6,7-dimethoxy-2-isoquinolinyl)ethyl]-phenyl)-9,10-dihydro-5-methoxy-9-oxo-4-acridine carboxamide; LSC, liquid scintillation counting; MCT, 0.5% methylcellulose with 0.2% Tween 80; MDCK, Madin-Darby canine kidney; MLP, maximum lifespan potential; mTOR, mammalian target of rapamycin; N.D., not determined; PBS, phosphate-buffered saline; PD, pharmacodynamics; PK, pharmacokinetics; QWBA, quantitative whole-body autoradiography; TV, tumor volume; MDR1, multidrug resistance 1; Bcrp1, breast cancer resistance protein 1.

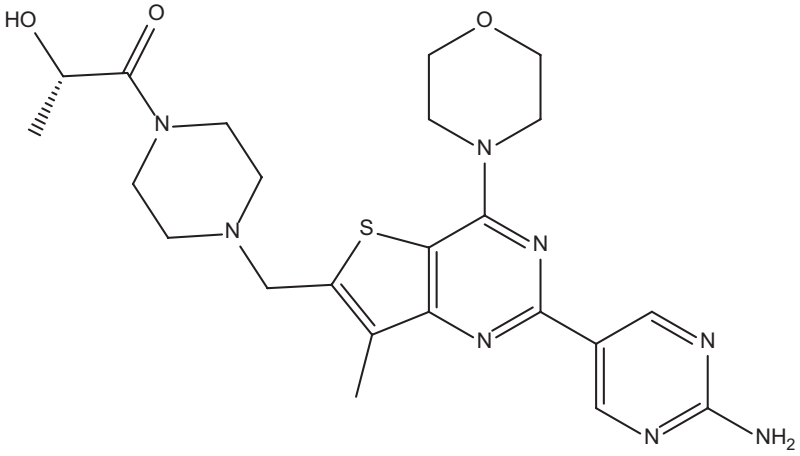

FIG. 1. Chemical structure of GDC-0980.

it is expected that the inhibition of both mTOR complexes would prevent PI3K pathway activation by this mechanism.

The implication of both PI3K and mTOR in cancer and the results obtained through their separate inhibition have led to the development of compounds able to inhibit both kinases, which are being tested currently (Liu et al., 2009a).

(*S*)-1-{4-[2-(2-Amino-pyrimidin-5-yl)-7-methyl-4-morpholin-4-yl-thieno[3,2-*d*]pyrimidin-6-ylmethyl]-piperazin-1-yl}-2-hydroxy-propan-1-one (GDC-0980) (Fig. 1) is a small molecule inhibitor of class I PI3K and mTOR (mTORC1 and mTORC2) that is being developed by Genentech, Inc. for the treatment of various malignancies. GDC-0980 was shown to be selective against a large panel of related kinases, including DNA-dependent protein kinase, VPS34, and c2alpha and c2beta (Castanedo et al., 2008), and can be considered equipotent against the four class I PI3K isoforms, with IC_{50} values of 0.005, 0.027, 0.007, and 0.014 μM against p110α, β, δ, and γ, respectively. In addition, it is a potent inhibitor of mTOR, with a K_i of 0.017 μM (Sutherlin et al., 2011). GDC-0980 also is able to inhibit the proliferation of MCF7-neo/HER2 breast and PC3-NCI prostate cancer cells with IC_{50} values of 0.24 and 0.12 μM, respectively, and was efficacious against these tumor cell lines grown as xenografts in immunocompromised mice (Sutherlin et al., 2011; Wallin et al., 2011).

The purposes of the present studies were to assess the absorption and disposition properties of GDC-0980 and to model its efficacy in the MCF7-neo/HER2 (breast, PI3K mutant) xenograft model. The results obtained in this preclinical evaluation were used to predict human GDC-0980 pharmacokinetic (PK) parameters and profile as well as its potential efficacy. When possible, these predictions were compared with the data from the Phase I study.

Materials and Methods

Chemicals and Reagents. GDC-0980 was synthesized at Genentech (South San Francisco, CA) and [^{14}C]GDC-0980 was synthesized at Selcia Limited (Essex, UK). All of the other reagents or materials used in these studies were purchased from Sigma-Aldrich (St. Louis, MO) unless otherwise stated.

In Vitro Studies. *Madin-Darby canine kidney cell permeability and transport studies.* The Madin-Darby canine kidney I (MDCKI) cell line, used in the permeability assay, was acquired from the American Type Culture Collection (Manassas, VA). For transport studies, MDR1-MDCKI cells were licensed from the National Cancer Institute (Bethesda, MD), whereas Bcrp1-MDCKII cells were obtained from the Netherlands Cancer Institute (Amsterdam, The Netherlands). The cells were seeded at a density of 1.3×10^5 cells/ml in Transwell plates (12-well, polyester membrane, 0.4-μm pore size, 1.0 cm^2 growth area; Corning Life Sciences, Lowell, MA) and cultured for 5 days at 37°C with 5% CO_2 and 95% humidity. GDC-0980 was tested at a concentration of 10 μM in the apical-to-basolateral (A-B) and basolateral-to-apical (B-A) directions. In the transfected cells, the studies were conducted in the absence and presence of *N*-(4-[2-(1,2,3,4-tetrahydro-6,7-dimethoxy-2-isoquinolinyl)ethyl]-phenyl)-9,10-dihydro-5-methoxy-9-oxo-4-acridine carboxamide (GF120918) (2 μM; inhibitor of P-gp) or fumitremorgin C (10 μM; inhibitor of Bcrp1). The compound was dissolved in transport buffer consisting of Hanks' balanced salt solution and 10 mM HEPES (Invitrogen, Carlsbad, CA). Transepithelial electrical resistance and lucifer yellow permeability were used to monitor monolayer integrity at the beginning and the end of the experiments, respectively. GDC-0980 was analyzed by liquid chromatography-tandem mass spectrometry (LC-MS/MS). The apparent permeability (P_{app}), in the A-B and B-A directions, was calculated as follows: $P_{app} = (dQ/dt)(1/AC_0)$, where dQ/dt is the rate of compound appearance in the receiver compartment, A is the surface area of the insert, and C_0 is the initial substrate concentration at T_0. The efflux ratio (ER) was calculated as $P_{app,B\text{-}A}/P_{app,A\text{-}B}$.

Metabolic stability study in cryopreserved hepatocytes. The metabolic stability of GDC-0980 was evaluated in pooled cryopreserved hepatocytes from CD-1 mice ($n = 10$ animals), Sprague-Dawley rats ($n = 3$ animals), cynomolgus monkeys ($n = 3$ animals), beagle dogs ($n = 3$ animals) (Invitrogen), and humans ($n = 10$; Celsis, Baltimore, MD). The cells were resuspended at a density of 0.5×10^6 cells/ml, and the reactions were initiated with the addition of GDC-0980 at a final concentration of 1 μM. Samples were incubated at 37°C in 5% CO_2 with saturating humidity, and aliquots were sampled at 0, 1, 2, and 3 h. Reactions were quenched with acetonitrile at each time point. The samples were centrifuged at 2000*g* for 10 min, the supernatant was diluted with water (1:2 ratio), and the percentage of GDC-0980 remaining was determined by LC-MS/MS. With the $t = 0$ peak area ratio values as 100%, the in vitro intrinsic clearance (CL) and scaled hepatic CL were determined as described by Obach et al. (1997).

Blood-to-plasma partitioning. The blood-to-plasma partitioning of GDC-0980 was assessed in pooled whole blood with K_2EDTA anticoagulant from CD-1 mice, Sprague-Dawley rats, beagle dogs, cynomolgus monkeys, and humans (Bioreclamation, Inc., Hicksville, NY). Blood from all of the species was obtained from at least three individual donors. GDC-0980 and [^{14}C]GDC-0980 were added to whole blood at total concentrations of 1, 10, and 40 μM. Blood samples were incubated at 37°C for 60 min in a shaking water bath. After the incubation, an aliquot of blood was sampled, and the remaining blood was centrifuged to obtain plasma. Radioactivity in plasma and blood was determined using a Packard Tri-Carb 2900TR liquid scintillation counter (PerkinElmer Life and Analytical Sciences, Waltham, MA). The blood-to-plasma ratio was calculated by dividing the measured radioactivity in blood by that measured in plasma. Incubations were performed in triplicate. Parameters are presented as mean ± S.D.

Plasma protein binding. The extent of plasma protein binding of GDC-0980 was determined in vitro, in CD-1 mouse, Sprague-Dawley rat, cynomolgus monkey, beagle dog, and human plasma (Bioreclamation, Inc.), by equilibrium dialysis using a 96-well block (HTDialysis LLC, Gales Ferry, CT). GDC-0980 and [^{14}C]GDC-0980 were added to pooled plasma ($n \geq 3$) at total concentra-

tions of 1, 10, and 40 μM. These concentrations were selected to cover the range of potential clinical levels and preclinical concentrations measured. Plasma samples were equilibrated with phosphate-buffered saline (PBS) (pH 7.4) at 37°C in 95% humidity and 5% CO_2 for 6 h. After the dialysis, radioactivity in plasma and buffer was measured using a Packard Tri-Carb 2900TR liquid scintillation counter. The percentage GDC-0980 unbound in plasma was determined by dividing the radioactivity measured in the postdialysis buffer by that measured in the postdialysis plasma and multiplying by 100. Incubations were performed in quadruplicate. Parameters are presented as mean ± S.D.

Brain tissue binding. The extent of brain tissue binding of GDC-0980 was determined in vitro, in CD-1 mouse brain (Bioreclamation, Inc.), using a Rapid Equilibrium Dialysis device (Thermo Fisher Scientific, Waltham, MA). Brain homogenate was prepared by homogenizing 1 g of brain with 3 ml of PBS (pH 7.4) using a BeadBeater (BioSpec Products, Bartlesville, OK). GDC-0980 was added to brain homogenate ($n = 3$) to a final concentration of 10 μM. Brain homogenate samples then were equilibrated with PBS at 37°C in 95% humidity and 5% CO_2 for 4 h at a shaking speed of 150 rpm. After the incubation, a quenching mixture containing an internal standard, blank PBS, or blank brain homogenate was added to the postdialysis PBS sample and postdialysis brain sample so that the matrices of both sides were equivalent. Samples were centrifuged, and the supernatants were analyzed using LC-MS/MS for GDC-0980 concentrations. Incubations were performed in triplicate. Calculations of the free fraction were performed as described by Kalvass et al. (2007). Parameters are presented as mean ± S.D.

In Vivo Studies. All of the studies performed were approved by the Institutional Animal Care and Use Committees at Genentech, Inc., Harlan Bioproducts for Science Inc. (Indianapolis, IN), Covance Laboratories Inc. (Madison, WI), Covance Research Products (Princeton, NJ), MPI Research, Inc. (Mattawan, MI), or QPS, LLC (Newark, DE). When GDC-0980 was administered orally, animals were fasted overnight until 4 h postdose.

Pharmacokinetic study in mouse. Twenty-seven female NCr nude mice (Taconic Farms, Germantown, NY) were given a 1 mg/kg intravenous bolus dose of GDC-0980 in 5% dimethyl sulfoxide with 5% cremophor. Three additional groups of 27 mice each received a 1, 5, or 10 mg/kg p.o. dose of GDC-0980 as a 0.5% methylcellulose with 0.2% Tween 80 (MCT) suspension. At the initiation of the study, the mice weighed from 16.5 to 26.9 g. One blood sample of approximately 0.2 ml was collected from each mouse ($n = 3$ mice per time point) by terminal cardiac puncture, while the animals were anesthetized with isoflurane. Blood samples were collected in tubes containing K_2EDTA as the anticoagulant, predose, and at 0.033, 0.16, 0.5, 1, 3, 6, 9, and 24 h after the intravenous administration, and predose and at 0.083, 0.25, 0.5, 1, 3, 6, 9, and 24 h after the oral dose. Samples were centrifuged within 30 min of collection, and plasma was collected and stored at −80°C until analysis. The concentration of GDC-0980 in each plasma sample was determined by LC-MS/MS analysis.

Pharmacokinetic study in rat. Three days before the study, jugular and femoral vein cannulae were implanted in male Sprague-Dawley rats (Charles River Laboratories, Inc., Wilmington, MA) assigned to the intravenous group, and only jugular vein cannulae were implanted in rats assigned to the oral group. At the initiation of the study, the rats weighed from 262 to 294 g. Three rats were given a single intravenous dose of 1 mg/kg GDC-0980 in 5% dimethyl sulfoxide with 5% cremophor via the femoral vein cannulae. Three additional rats were given a single oral dose of 5 mg/kg GDC-0980 in 80% (w/v) polyethylene glycol 400 in water as a solution. Blood samples (approximately 0.2 ml per sample) were drawn from each animal via the jugular vein cannulae predose and at 0.033, 0.083, 0.25, 0.5, 1, 2, 4, 8, and 24 h postdose. Plasma samples were collected and analyzed as described above.

Pharmacokinetic study in monkey. Three male cynomolgus monkeys (Harlan Bioproducts for Science Inc.) were given GDC-0980 in a crossover study. The two phases were separated by a 7-day washout period. In the first phase of the study, monkeys were given a single intravenous dose of 1 mg/kg of GDC-0980 in 30% hydroxypropyl-β-cyclodextrin solution via a saphenous vein. In the second phase, the same monkeys each were given a single oral dose of 2 mg/kg GDC-0980 as an MCT suspension via nasogastric intubation. At the initiation of the study, the monkeys weighed from 2.29 to 3.32 kg. Blood samples (approximately 1 ml per sample) were collected predose and at 0.033, 0.083, 0.25, 0.5, 1, 2, 4, 8, 12, and 24 h after the intravenous dose and predose and at 0.083, 0.25, 0.5, 1, 2, 4, 8, 12, and 24 h after the oral dose. Plasma was isolated within 1 h of blood collection and stored at −80°C until analysis. Urine was collected overnight predose and 0 to 24 h postdose from the animals receiving the intravenous dose. Urine volume was measured and recorded. A 10-ml aliquot of urine for each sample (when available) was taken from the bulk and was stored at −80°C until analysis. The concentration of GDC-0980 in each plasma and urine sample was determined using an LC-MS/MS assay.

Pharmacokinetic study in dog. Six male beagle dogs (9.1 to 13.2 kg; Harlan Bioproducts for Science Inc.) were given GDC-0980 in a parallel study. The first group of three dogs received a single intravenous dose of 1 mg/kg GDC-0980 in 30% hydroxypropyl-β-cyclodextrin solution via a cephalic vein. The second group of three dogs each received a 2 mg/kg p.o. dose of GDC-0980 as an MCT suspension. Blood samples (approximately 3 ml per sample) were collected predose and at 0.033, 0.083, 0.25, 0.5, 1, 2, 4, 8, 12, and 24 h after the intravenous dose and predose and at 0.083, 0.25, 0.5, 1, 2, 4, 8, 12, and 24 h after the oral dose. Blood and plasma were processed as described above.

LC-MS/MS Analysis. GDC-0980 plasma and urine concentrations were determined by LC-MS/MS using a nonvalidated method. After plasma protein precipitation with acetonitrile, the supernatant was injected onto the column, a Gemini C18 column (30 × 2 mm, 5 μm particle size; Phenomenex, Torrance, CA). A CTC HTS PAL autosampler (LEAP Technologies, Carrboro, NC) linked to a SCL-10A controller with LC-10AD pumps (Kyoto, Japan), coupled with an API 4000 triple quadrupole mass spectrometer (Applied Biosystems/MDS Sciex, Foster City, CA) were used for the LC-MS/MS assay. The aqueous mobile phase was water with 0.1% formic acid, and the organic mobile phase was acetonitrile with 0.1% formic acid (B). The gradient was as follows: 10% B for the first 0.5 min, increased to 90% B from 0.5 to 2 min, maintained at 90% B for 1.5 min, and decreased to 10% B within 0.1 min. The total run time was 5 min with a flow rate of 0.5 ml/min, and the ionization was conducted in the positive ion mode using the transition m/z 499.3 → 341.1 in atmospheric pressure chemical ionization mode. GDC-0980 retention time was 1.2 min. The injection volume was 20 μl. The lower and upper limits of quantitation of the assay were 0.005 and 10 μM, respectively. The internal standard for the plasma and urine assays was the deuterated (d_8) analog (dog and monkey studies) or a closely related analog (mouse and rat studies) of GDC-0980.

Pharmacokinetic Analysis. Pharmacokinetic parameters were calculated by noncompartmental methods as described by Gibaldi and Perrier (1982) using WinNonlin (version 5.2; Pharsight, Mountain View, CA). Parameters are presented as mean ± S.D. Bioavailability (F) in monkeys was determined for each animal by dividing the dose-normalized area under the plasma concentration-time curve extrapolated to infinity (AUC_{inf}) obtained after each oral dose by the dose-normalized AUC_{inf} obtained after the intravenous dose. In dogs, rats, and mice, F was determined by dividing the dose-normalized AUC_{inf} for each animal dosed orally by the dose-normalized mean AUC_{inf} determined from the animals dosed intravenously (a pooled profile was used in mice). Renal clearance was estimated in monkeys after the intravenous dose by dividing the cumulative amount of GDC-0980 excreted over the 24-h urine collection period by plasma AUC_{0-24} obtained after the intravenous dose.

Mass balance and routes of elimination in rat. A single oral dose of [^{14}C]GDC-0980 (2 mg/kg; 100 μCi/kg) was administered to bile duct-intact and bile duct-cannulated (BDC) male and female Sprague-Dawley rats ($n = 3$ per sex; Covance Laboratories Inc.). The dose was prepared in MCT. Urine and feces were collected from the bile duct-intact rats in plastic containers surrounded by dry ice predose (overnight for at least 12 h) and at 0 to 8 and 8 to 24 h postdose and at 24-h intervals through 168 h postdose. Urine and bile were collected from BDC animals in plastic containers surrounded by dry ice predose (overnight for at least 12 h) and at 0 to 8 and 8 to 24 h postdose and at 24-h intervals through 120 h postdose. All of the samples were stored at approximately −70°C before and after analysis.

Urine, bile, cage rinse, and cage wash samples were mixed by shaking, and aliquots were analyzed directly by liquid scintillation counting (LSC). Feces samples were mixed with a sufficient amount of solvent (ethanol/water, 1:1, v/v) to facilitate homogenization, and aliquots were combusted and analyzed by LSC. All of the samples were analyzed in duplicate if sample size allowed.

All of the sample combustions were done in a model 307 sample oxidizer (PerkinElmer Life and Analytical Sciences), and the resulting $^{14}CO_2$ was

trapped in a mixture of Permafluor and Carbo-Sorb (PerkinElmer Life and Analytical Sciences). Ultima Gold XR scintillation cocktail was used for samples analyzed directly. All of the samples were analyzed for radioactivity in Packard Tri-Carb 2900TR liquid scintillation counters for at least 5 min or 100,000 counts.

Mass balance and routes of elimination in dog. A single dose of [^{14}C]GDC-0980 at a target dose of 2 mg/kg (20 μCi/kg) was administered to two male and two female bile duct-intact and two male BDC beagle dogs (MPI Research, Inc., Mattawan, MI). The dose prepared with both radiolabeled and nonradiolabeled GDC-0980 in MCT was administered via oral gavage at a dose volume of 5 ml/kg. Urine and feces were collected in plastic containers (surrounded by dry ice for urine only) predose and at 0 to 8 and 8 to 24 h postdose and at 24-h intervals through 240 h postdose. Bile was collected from BDC animals in plastic containers surrounded by dry ice predose and at 0 to 8 and 8 to 24 h postdose and at 24-h intervals through 168 h postdose. For urine and bile, triplicate aliquots (approximately 0.5 and 0.2 g, respectively) were weighed into glass scintillation vials, and an appropriate amount of Ultima Gold LSC cocktail (PerkinElmer Life and Analytical Sciences) was added before direct analysis by LSC. For feces, the appropriate amount of deionized water was added to the samples to create a 4:1 homogenate. Triplicate aliquots (approximately 0.5 g) were weighed into combustion cones and oxidized by combustion. The required amounts of Carbo-Sorb E and Permafluor E+ were added to the oxidized aliquots before the analysis by LSC. For cage rinses, triplicate aliquots (approximately 1 g each) were weighed into glass scintillation vials, and appropriate amounts of Ultima Gold LSC cocktail were added before the analyses by LSC. All of the radioactive samples collected were counted by LSC for at least 5 min or 100,000 counts in triplicate, sample size allowing.

Quantitative whole-body autoradiography in rats. The tissue distribution of [^{14}C]GDC-0980-related radioactivity in Sprague-Dawley rats (Hilltop Laboratory Animals, Inc., Scottdale, PA) was investigated after a single oral dose of 2 mg/kg (100 μCi/kg) in MCT using whole-body autoradiography. Animals were euthanized at 1, 8, 24, and 120 h postdose. The carcasses were frozen in hexane dry ice and stored at −20°C before processing for quantitative whole-body autoradiography (QWBA). Each carcass was embedded, cut into sagittal sections, and mounted for QWBA. Selected sections were exposed to phosphor image screens, and tissue radioactivity concentrations were quantified from the whole-body autoradiograms using an image analysis system [Typhoon 9410 image acquisition system (GE Healthcare, Little Chalfont, Buckinghamshire, UK); MCID image analysis software, version 7.0; GE Healthcare]. Concentrations of radioactivity were expressed as μCi/g and converted to microgram equivalents of GDC-0980 per gram of matrix (μg equiv/g) using the specific activity (47.1 μCi/mg) of the administered formulated [^{14}C]GDC-0980.

Studies in FVBn and Mdr1a/b(−/−)/Bcrp1(−/−) mice. Male FVBn (wild-type) and *Mdr1a/b(−/−)/Bcrp1(−/−)* mice were obtained from Taconic Farms (Germantown, NY). The mice weighed between 19 and 28 g at the beginning of the study. GDC-0980, prepared in MCT, was administered by oral gavage at a dose volume of 10 ml/kg. The animals received 20 mg/kg p.o. GDC-0980. Blood samples (0.2 ml) were collected 1 and 6 h postdose. Samples were taken from three mice at each time point. Each mouse was sampled twice (retro-orbital collection and cardiac puncture). After being mixed with K_2EDTA (anticoagulant), the blood samples were stored on ice and, within 1 h of collection, were centrifuged at 2000*g* for 5 min at 2 to 8°C. Plasma was collected and stored at −80°C until analysis. Total concentrations of GDC-0980 were determined by LC-MS/MS. Brains also were collected at 1 and 6 h postdose from three mice at each time point. Each brain was rinsed with ice-cold saline, blotted dry, and cut into two halves along the sagittal plane for GDC-0980 concentration measurement and pharmacodynamic (PD) analysis. Each half of the brain was weighed, then snap-frozen in liquid nitrogen, and stored at −80°C until analysis. The right halves of the brains were homogenized in three volumes of water. The homogenates were extracted by protein precipitation with acetonitrile containing the internal standard and then analyzed by LC-MS/MS. Brain homogenate concentrations were converted to brain concentrations for the calculations of brain-to-plasma ratios. The internal standard for the plasma and brain assays was the deuterated (d_8) analog of GDC-0980.

For PD analysis, cell extraction buffer (Invitrogen) containing 10 mM Tris (pH 7.4), 100 mM NaCl, 1 mM EDTA, 1 mM EGTA, 1 mM NaF, 20 mM $Na_4P_2O_7$, 2 mM Na_3VO_4, 1% Triton X-100, 10% glycerol, 0.1% SDS, and 0.5% deoxycholate was supplemented with phosphatase, protease inhibitors (Sigma-Aldrich), and 1 mM phenylmethylsulfonyl fluoride and added to frozen brain biopsies. Brains were homogenized with a small pestle (Konte Glass Company, Vineland, NJ), sonicated briefly on ice, and centrifuged at 20,000*g* for 20 min at 4°C. Protein concentration was determined using a bicinchoninic acid protein assay (Thermo Fisher Scientific). Proteins were separated by electrophoresis and transferred to NuPAGE nitrocellulose membranes (Invitrogen). An Odyssey infrared detection system (LI-COR Biosciences, Lincoln, NE) was used to assess and quantify protein expression. PI3K and mTOR pathway markers were evaluated by immunoblotting using antibodies against pAkt^{Ser473}, total Akt, pS6$^{Ser235/236}$, and total S6 (Cell Signaling Technology, Danvers, MA). Inhibition (%) of pAkt and pS6 in wild-type and triple-knockout mice treated with GDC-0980 was calculated by comparing pAkt and pS6 signal with that measured in untreated mice.

MCF7-neo/HER2 Breast Cancer Xenograft Studies. The MCF7-neo/HER2 cell line was developed at Genentech, Inc. by expressing human HER2

TABLE 1

Apparent permeability (P_{app}) of GDC-0980 in MDCK, MDR1-MDCK, and Bcrp1-MDCK cells

Results reported as mean of duplicate.

Cell Line	P_{app}		P_{app} Ratio
	A to B	B to A	B-A/A-B
	10^{-6} cm/s		
MDCKI	18	30	1.7
MDR1-MDCKI	1.0	19	19
MDR1-MDCKI + GF120918	17	19	1.1
Bcrp1-MDCKII	0.93	6.2	6.7
Bcrp1-MDCKII + Fumitremorgin C	8.1	6.0	0.74

TABLE 2

Hepatic clearance of GDC-0980 in multiple species predicted from hepatocyte incubations

Results reported as mean of duplicate.

Species	Predicted Hepatic CL
	$ml \cdot min^{-1} \cdot kg^{-1}$
Mouse	5.1
Rat	3.3
Monkey	9.7
Dog	3.8
Human	3.3

TABLE 3

Blood-to-plasma ratio of [^{14}C] GDC-0980 in mouse, rat, dog, monkey, and human whole blood

Results reported as mean ± S.D. (n = 3).

Species	Total GDC-0980 Concentration[a]	Blood-Plasma Ratio of [^{14}C]GDC-0980
	μM	
Mouse	1	0.75 ± 0.016
	10	0.78 ± 0.049
	40	0.85 ± 0.041
Rat	1	0.97 ± 0.017
	10	0.92 ± 0.045
	40	0.90 ± 0.027
Cynomolgus monkey	1	1.1 ± 0.0043
	10	1.1 ± 0.035
	40	1.0 ± 0.0087
Dog	1	0.94 ± 0.039
	10	0.85 ± 0.013
	40	0.83 ± 0.0042
Human	1	1.3 ± 0.015
	10	1.1 ± 0.081
	40	1.1 ± 0.055

[a] Unlabeled and ^{14}C-labeled GDC-0980.

TABLE 4

Percentage of [^{14}C] GDC-0980 free in mouse, rat, dog, monkey, and human plasma

Results reported as mean ± S.D. (n = 4).

Species	Total GDC-0980 Concentration[a]	Free [^{14}C]GDC-0980
	μM	%
Mouse	1	29 ± 3.1
	10	29 ± 2.6
	40	32 ± 1.2
Rat	1	42 ± 3.5
	10	41 ± 2.9
	40	42 ± 0.94
Dog	1	49 ± 1.8
	10	52 ± 2.4
	40	52 ± 1.1
Cynomolgus monkey	1	46 ± 3.8
	10	48 ± 1.5
	40	51 ± 1.9
Human	1	39 ± 2.8
	10	41 ± 0.29
	40	45 ± 2.6

[a] Unlabeled and ^{14}C-labeled GDC-0980.

in the MCF7 human breast cancer cell line (American Type Tissue Collection, Manassas, VA).

Because the tumorigenicity of the MCF7-neo/HER2 cells in mice is estrogen dependent, estrogen pellets (17β-estradiol, 0.36 mg/pellet, 60-day release) obtained from Innovative Research of America, Inc. (Sarasota, FL) were implanted into the dorsal shoulder blade area of female NCr nude mice. After 3 to 7 days, 20 million human breast cancer MCF7-neo/HER2 cells, resuspended in a 1:1 mixture of Hanks' balanced salt solution and Matrigel basement membrane matrix (BD Biosciences, San Jose, CA), were implanted subcutaneously into the right flank of each mouse. After the implantation, tumors were monitored until they reached a mean tumor volume (TV) of 200 to 300 mm^3. Tumor size and body weight were recorded twice per week during the study. Animal body weights were measured using an Adventurer Pro AV812 scale (Ohaus Corporation, Pine Brook, NJ). Tumor lengths and widths were measured using Ultra-Cal IV calipers (model 54-10-111, Fred V. Fowler Company, Inc., Newton, MA). Mice were euthanized if body weight loss was >20% from their initial body weight or if the tumors exceeded 2000 mm^3. The mean TV across all of the groups was 226 mm^3 at the initiation of dosing. Ten mice were assigned to each dose group.

TV was calculated using the following equation with Excel (version 11.2; Microsoft, Redmond, WA): TV (mm^3) = length × width^2 × 0.5.

GDC-0980 was administered orally in MCT for 21 days. Animals in the control groups received the vehicle, MCT (100 μl). The animals treated with GDC-0980 received the following doses in 100 μl of MCT: 0.25, 0.5, 1, 2.5, 5, and 7.5 mg/kg once daily. The TVs at the end of the study for each group were compared with the TVs of the vehicle group.

Pharmacokinetic-Pharmacodynamic Modeling. PK and PK-PD modeling was performed using SAAM II (SAAM Institute, University of Washington, Seattle, WA).

Pharmacokinetic analysis. A one-compartment model with first-order oral absorption was used to fit the mean plasma concentration-time data from female NCr nude mice. The pharmacokinetics of GDC-0980 appeared linear over the range of doses tested, and the three single doses (1, 5, and 10 mg/kg) were fitted simultaneously. The mean estimates of the absorption rate constant (k_a), the elimination rate constant (k_e), and the apparent volume of distribution

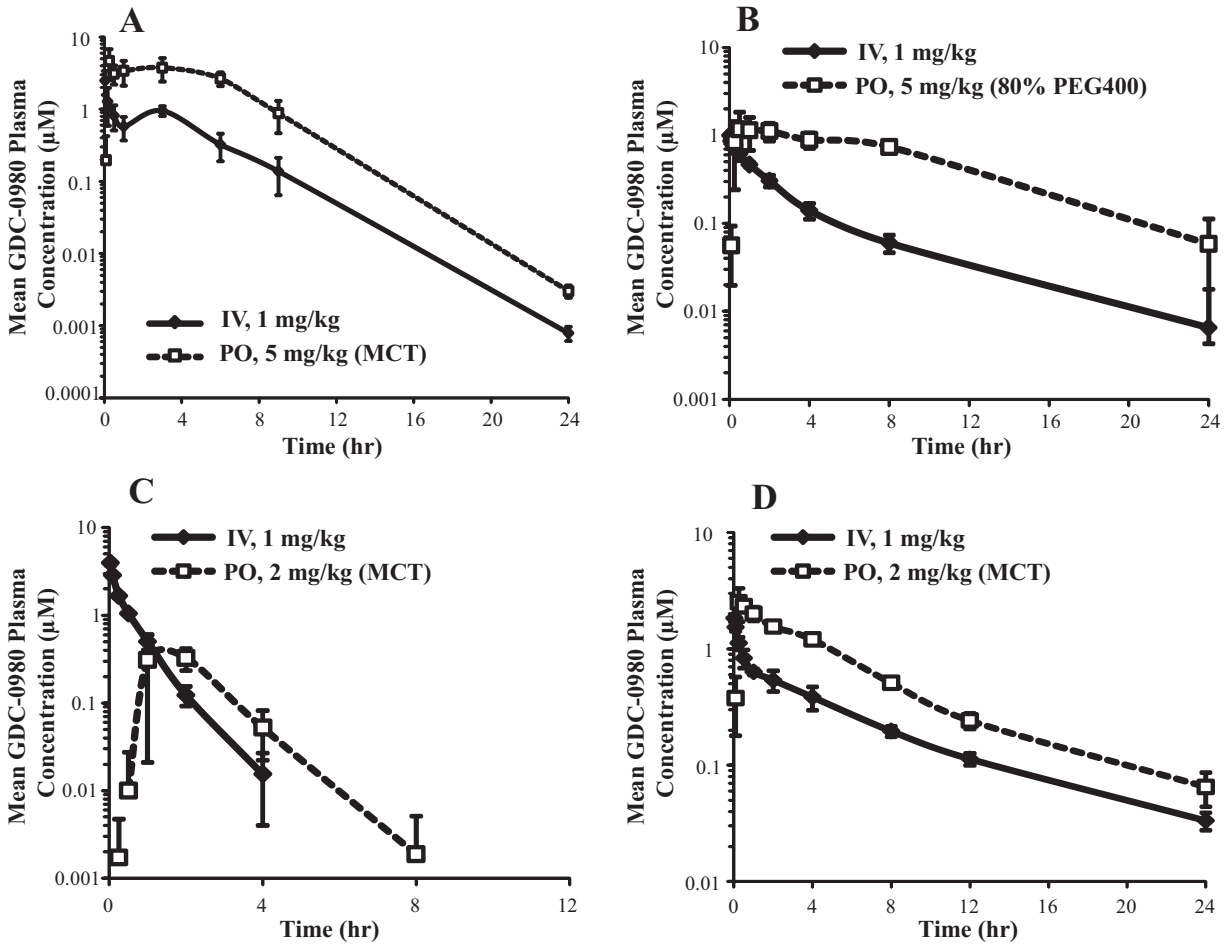

FIG. 2. Mean plasma concentration-time profiles after intravenous (1 mg/kg) and oral (5 mg/kg in rodents; 2 mg/kg in monkey and dog) administrations of GDC-0980. A, mouse; B, rat; C, cynomolgus monkey; D, dog. Error bars represent S.D.

TABLE 5

Pharmacokinetic parameters (mean ± S.D.) of GDC-0980 in mouse, rat, dog, and monkey after intravenous and oral administrations

Parameters	NCr Nude Mice	Sprague-Dawley Rats	Beagle Dogs	Cynomolgus Monkeys
No. of animals	27* (3/time point)	3*	3†	3†
Sex	Female	Male	Male	Male
Dose, mg/kg	1	1	1	1
CL, ml · min^{-1} · kg^{-1}	6.30	15.4 ± 2.85	6.38 ± 0.657	19.0 ± 1.31
$t_{1/2}$, h	2.05	3.52 ± 2.39	6.41 ± 0.885	0.558 ± 0.101
Mean residence time, h	3.84	4.38 ± 2.50	7.57 ± 0.780	0.654 ± 0.106
V_{ss}, l/kg	1.45	3.78 ± 1.43	2.90 ± 0.397	0.739 ± 0.0678
Renal clearance, ml · min^{-1} · kg^{-1}	N.D.	N.D.	N.D.	0.405 ± 0.268
Oral administration				
No. of animals	27§ (3/time point)	3‡	3§	3§
Sex	Female	Male	Male	Male
Dose, mg/kg	5	5	2	2
AUC_{inf}, μM·h	26.9	11.8 ± 3.31	13.2 ± 0.545	0.813 ± 0.302
C_{max}, μM	4.65	1.31 ± 0.533	2.71 ± 0.524	0.438 ± 0.184
t_{max}, h	0.25	1.17 ± 0.764	0.333 ± 0.144	1.67 ± 0.577
F, %	101	106 ± 29.7	125 ± 5.16	22.9 ± 8.56

N.D., not determined.
* Doses prepared in 5% dimethyl sulfoxide and 5% cremophor in water.
† Doses prepared in 30% hydroxypropyl-β-cyclodextrin.
‡ Doses prepared in 80% polyethylene glycol 400 in water.
§ Doses prepared in 0.5% methylcellulose with 0.2% Tween 80.

(*V*/*F*) were used to simulate the GDC-0980 plasma concentrations for the modeling of the xenograft efficacy study.

Xenograft efficacy study. An indirect response model, described by differential eq. 1, was fitted to the xenograft efficacy data.

$$\frac{d(TV)}{dt} = k_{ng}(TV) - K\,(TV) \quad (1)$$

where *t* is time (h), TV is the tumor volume (mm^3), k_{ng} is the net growth rate constant (h^{-1}), and *K* is the rate constant (h^{-1}) associated with the reduction of tumor by GDC-0980. *K* is described further as eq. 2:

$$K = \frac{K_{max} \times C^n}{KC_{50}^n + C^n} \quad (2)$$

where K_{max} is the maximum value of *K* (h^{-1}), *C* is the plasma concentration of GDC-0980 (μM), *n* is the Hill coefficient, and KC_{50} is the concentration of GDC-0980 where *K* is 50% of K_{max}.

GDC-0980 plasma concentrations in mice were simulated based on the parameters determined in the pharmacokinetic studies, and mean TVs from each dose group were used in the modeling. The ED_{60} was determined by fixing PD parameter estimates and simulating the daily dose required for a 60% reduction of the TV relative to that of the vehicle control group at the end of the study. The plasma concentration needed to achieve tumor stasis was determined when *K* was equal to k_{ng}.

Prediction of Human PK Parameters and Efficacious Doses. Human volume of distribution and plasma CL were predicted using simple allometric scaling and incorporating the "rule of exponents" (Mahmood and Balian, 1996) for CL prediction. In vivo CL and volume of distribution at steady-state (V_{ss}) estimated in preclinical species were scaled as a function of body weight using the following power function (allometric equation): $Y = aW^b$, where *Y* is CL × MLP, or volume of distribution, *W* is the body weight, and *a* and *b* are the allometric coefficient and exponent, respectively. MLP is the maximum lifespan potential, as described by Boxenbaum (1982). Body weights of 0.02, 0.25, 3, and 10 kg were used for mouse, rat, monkey, and dog, respectively. Predicted human CL and V_{ss} were extrapolated assuming a body weight of 70 kg.

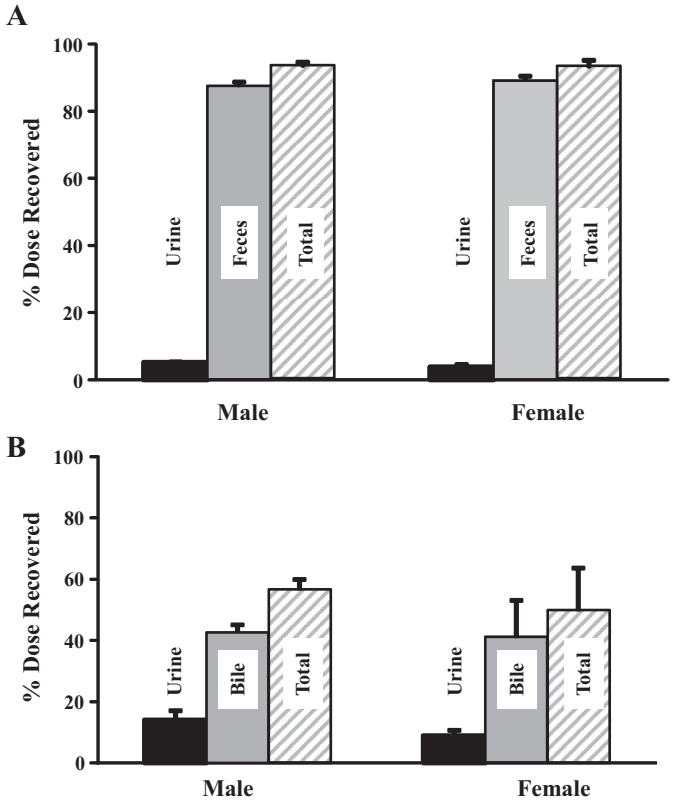

FIG. 3. Recovery of [^{14}C]GDC-0980-related radioactivity after oral administration of 2 mg/kg (100 μCi/kg) of GDC-0980 to male and female bile duct-intact (A) and BDC (B) Sprague-Dawley rats. Results presented as mean ± S.D. (n = 3 rat/sex).

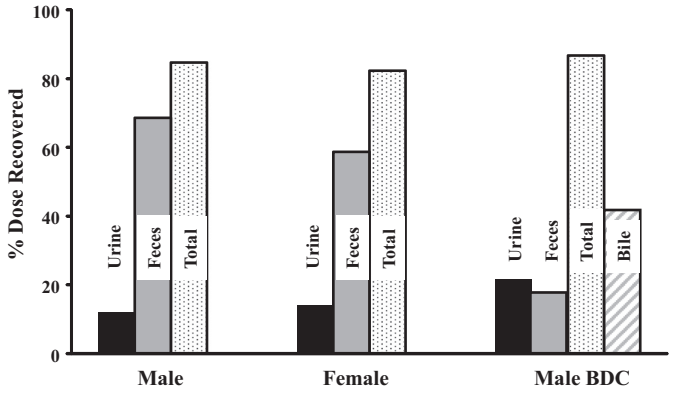

FIG. 4. Recovery of [^{14}C]GDC-0980-related radioactivity after oral administration of 5 mg/kg (20 μCi/kg) of GDC-0980 to male and female bile duct-intact and BDC beagle dogs. Results presented as mean of two animals.

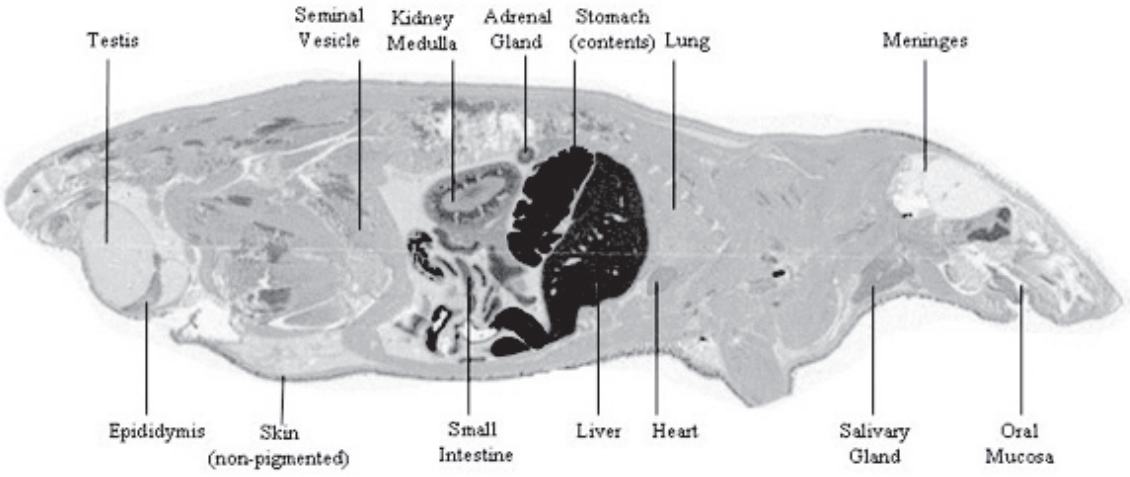

FIG. 5. Whole-body autoradiogram of the radioactivity distribution in a male Sprague-Dawley rat at 1 h after a single oral administration of [14C]-GDC-0980 at a target dose of 2 mg/kg (200 μCi/rat).

Human PK profile simulations using GastroPlus. The PBPKPlus module of the GastroPlus simulation software (Simulations Plus, Lancaster, CA) was used to predict the PK profile of GDC-0980 in human, based on the physicochemical properties of the compound, its permeability (determined in MDCK cells and converted to a human P_{eff} of 1.34×10^{-4} cm/s), and the predicted CL from allometric scaling incorporating the MLP correction. The solubility profile (at pHs ranging from 2.3 to 10), Log *P* (2.02), and pK_a (3.1 and 4.8) were determined experimentally. The inputs for plasma protein binding (F_{up} = 42%) and blood-plasma partitioning (1.1) were those presented in this article. For all of the other parameters, the default settings of GastroPlus were used. The plasma concentration-time profile and PK parameters simulated with a dose of 2 mg (starting dose in Phase I) were compared with those obtained in patients (Wagner et al., 2009; Bendell et al., 2010). The simulated profile was fitted subsequently with a one-compartment model with first-order oral absorption using WinNonlin.

The human dose associated with 60% tumor growth inhibition compared with vehicle control was simulated based on the pharmacodynamic parameters estimated in the MCF7-neo/HER2 breast tumor xenograft model and substituting the mouse PK parameters with the human parameters derived from the simulated human profile. Simulations were performed using SAAM II.

TABLE 6

Concentrations of radioactivity (microgram equivalents of GDC-0980 per gram of sample) in tissues of male rats after a single oral dose of [^{14}C]GDC-0980 at 2 mg/kg

Tissue	Time after Compound Administration			
	1 h	8 h	24 h	120 h
Blood (in heart)	1.71	BQL	BQL	BQL
Bile (in duct)	77.3	7.23	6.34	BQL
Kidney cortex	8.73	0.316	0.320	BQL
Kidney medulla	8.50	0.360	0.382	BQL
Liver	23.9	2.17	1.95	0.183
Urinary bladder	3.52	0.170	BQL	BQL
Brain (cerebrum)	0.151	BQL	BQL	BQL
Brain (cerebellum)	BQL	BQL	BQL	BQL
Brain (medulla)	0.165	BQL	BQL	BQL
Spinal cord	0.139	BQL	BQL	BQL
Cecum	13.9	9.01	1.62	BQL
Large intestine	5.70	3.73	1.22	BQL
Small intestine	64.4	1.09	0.805	BQL
Skeletal muscle	3.750	BQL	BQL	BQL

BQL, below quantitation limit (0.120 μg equivalent/g tissue).

Results

Permeability and Transport in MDCK Cells. The apparent permeability (P_{app}) of GDC-0980 as assessed in parental MDCKI cells was high (Table 1) and comparable with that determined for metoprolol, the high P_{app} marker used in the same experiment (E. G. Plise, unpublished observations). The ER ($P_{app,B\text{-}A}/P_{app,A\text{-}B}$) was low (1.7), suggesting minor involvement of efflux transporter(s) in the B-A direction in this cell line. In contrast, when bidirectional transport was studied in MDR1-MDCK and Bcrp1-MDCKII cells, the ERs were 19 and 6.7, respectively. In the presence of the P-gp and Bcrp1 inhibitors, GF120918 and fumitremorgin C, these ERs were reduced to 1.1 and 0.74, respectively, confirming that GDC-0980 was a substrate of both transporters.

Metabolic Stability Study in Cryopreserved Hepatocytes. The hepatic CL predicted from the metabolic stability after a 3-h incubation in cryopreserved hepatocytes is presented in Table 2. Predicted hepatic CL was low in all of the species tested (<30% of hepatic blood flow) (Davies and Morris, 1993).

In Vitro Blood-to-Plasma Partitioning, Plasma Protein Binding, and Brain Tissue Binding. The mean blood-to-plasma partitioning of GDC-0980 in mouse, rat, cynomolgus monkey, dog, and human pooled whole blood ranged from 0.75 to 1.3 and appeared concentration independent from 1 to 40 μM (Table 3).

Protein binding for GDC-0980 was low in the five species tested, with the free fraction ranging from approximately 29% in mouse plasma to 52% in dog plasma (Table 4). Protein binding was independent of the concentration in the concentration range of 1 to 40 μM. Binding to mouse brain tissue measured at 10 μM GDC-0980 was 92.1 $\pm$ 2.4%.

Pharmacokinetics of GDC-0980 in Mouse, Rat, Monkey, and Dog. The semilog plots of GDC-0980 plasma concentration versus time for mouse, rat, monkey, and dog after intravenous and oral administrations are presented in Fig. 2. The pharmacokinetic parameters are presented in Table 5. GDC-0980 had low plasma CL (<30% of hepatic blood flow) in mice, rats, and dogs (6.30, 15.4, and 6.38 ml $\cdot$ min^{-1} $\cdot$ kg^{-1}, respectively) and a moderate plasma CL (approximately 43% of hepatic blood flow) of 18.9 ml $\cdot$ min^{-1} $\cdot$ kg^{-1} in monkeys. Terminal half-life values ranged from 0.558 h in monkey to 6.41 h in dog. The V_{ss} was moderate to high in all of the species, corresponding to approximately 1.1- to 5.6-fold total body water.

TABLE 7

Plasma and brain concentrations in wild-type and knockout mice after oral (20 mg/kg) administration of GDC-0980

Results presented as mean of three animals ± S.D.

Mice	Time	Total			Free		
		Brain	Plasma	Brain-to-Plasma Ratio	Brain	Plasma	Brain-to-Plasma Ratio
	h	*μM*	*μM*		*μM*	*μM*	
FVBn	1	0.52 ± 0.055	6.4 ± 1.1	0.082 ± 0.0087	0.042 ± 0.0044	1.9 ± 0.32	0.022 ± 0.0023
Mdr1a/1b(−/−)/Bcrp1(−/−)	1	9.9 ± 5.2	9.5 ± 4.6	1.0 ± 0.20	0.78 ± 0.41	2.8 ± 1.3	0.27 ± 0.054
FVBn	6	0.83 ± 0.31	10 ± 2.9	0.081 ± 0.0071	0.065 ± 0.024	2.9 ± 0.84	0.021 ± 0.0020
Mdr1a/1b(−/−)/Bcrp1(−/−)	6	10 ± 2.8	10 ± NC	1.1 ± NC	0.79 ± 0.23	2.9 ± NC	0.30 ± NC

NC, not calculated; $n = 2$.

Bioavailability after oral administration ranged from 22.9% in monkey to 125% in dog. The renal CL of GDC-0980 was assessed in monkey and was negligible, representing <3% of the plasma CL.

Mass Balance and Routes of Elimination in Rat. The excretion of radioactivity was determined after the administration of a single oral dose of [^{14}C]GDC-0980 (2 mg/kg) to bile duct-intact and BDC male and female Sprague-Dawley rats. [^{14}C]GDC-0980-derived radioactivity was excreted rapidly after oral administration to bile duct-intact male and female rats, primarily within the first 48 h after dosing (87.1 to 88.9% of the administered dose in males and females, respectively; L. Salphati, unpublished observations). Routes and rates of excretion were similar in both males and females. A high percentage of radioactivity was recovered in feces (87.5% in males and 89.1% in females; Fig. 3A). Approximately 42.6 to 41.1% of the administered radioactivity was recovered in the bile of male and female BDC rats through 120 h postdose (Fig. 3B). The combined recovery in urine and bile indicated that a minimum of 57 and 50% of the oral dose was absorbed, in males and females, respectively.

Mass Balance and Routes of Elimination in Dog. [^{14}C]GDC-0980-derived radioactivity recovered in feces accounted for 68.6 and 58.7% of the administered dose in male and female bile duct-intact dogs, respectively. Totals of 12.2 and 14.1% of the dose were recovered in urine from bile duct-intact male and female dogs, respectively (Fig. 4). After oral administration of [^{14}C]GDC-0980 to male BDC dogs, the mean fecal, urinary, and biliary recoveries were 17.8, 21.6, and 41.7%, respectively, of the administered dose. The combined biliary and urinary radioactivity recoveries suggested that a minimum of approximately 63% of the oral dose was absorbed.

QWBA in Rats. The tissue distribution of ^{14}[C]GDC-0980 was determined in male Sprague-Dawley rats using whole-body autoradiography at 1, 8, 24, and 120 h after oral administration. Compound-derived radioactivity was absorbed rapidly, with concentrations detected in all of the tissues at 1 h (Fig. 5; Table 6). Radioactivity levels were below the limit of quantitation at 24 h postdose for all of the tissues except the gastrointestinal tract and excretory tissues. Tissues with the highest radioactivity included the liver, kidney, and intestine.

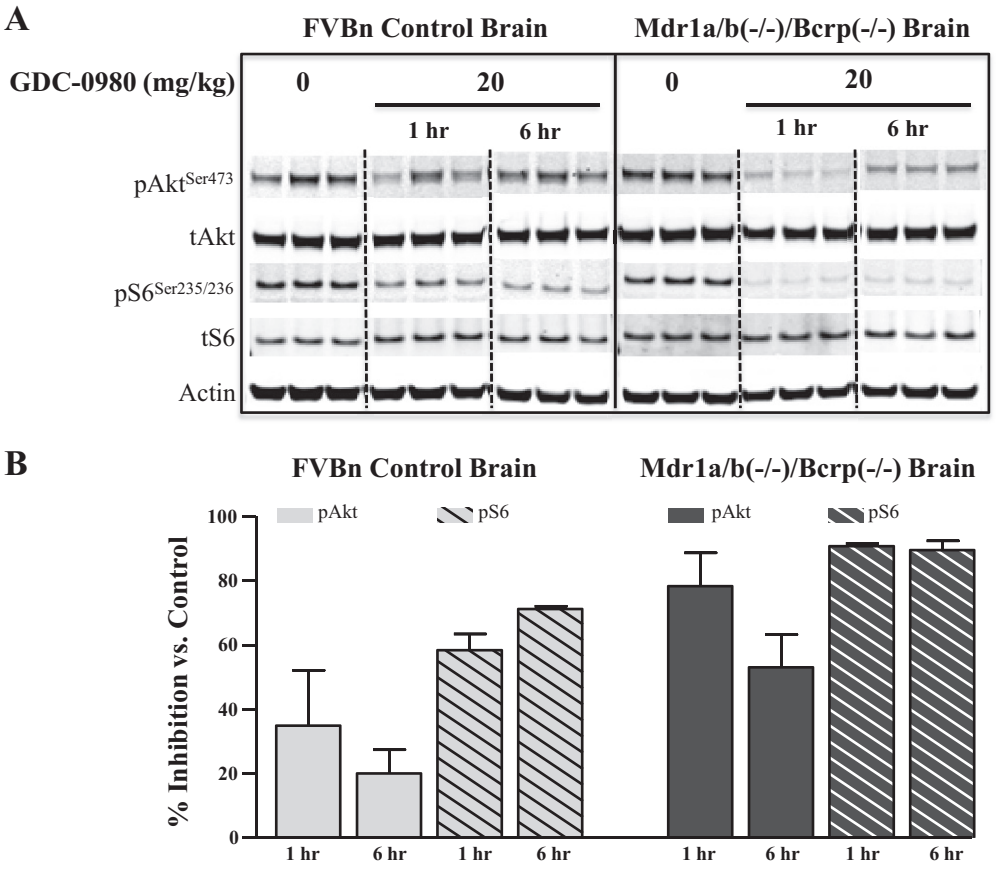

FIG. 6. Modulation of pAkt and pS6 in the brains of wild-type and *Mdr1a/b(−/−)/Bcrp1(−/−)* mice after oral administration of GDC-0980 at 20 mg/kg. A, Western blot of mouse brains probed with antibodies against pAkt, total Akt, pS6, total S6, and actin. B, quantitation of mean pAkt and pS6 inhibition at 1 and 6 h postdose in wild-type and *Mdr1a/b(−/−)/Bcrp1(−/−)* triple-knockout mice. Results are presented as the mean of three animals ± S.D.

High levels of radioactivity measured in the bile suggested that this was a major route of elimination. The lowest levels of radioactivity were measured in the brain and spinal cord (Table 6).

Studies in *Mdr1a/b(−/−)/Bcrp1(−/−)* and FVBn Mice. GDC-0980 was administered orally (20 mg/kg) to FVBn and *Mdr1a/b(−/−)/Bcrp1(−/−)* mice. Concentrations measured in plasma and brains were comparable between 1 and 6 h postdose in each strain of mice. Plasma concentrations were also similar between FVBn and *Mdr1a/b(−/−)/Bcrp1(−/−)* mice at the two time points (Table 7). In contrast, brain concentrations were 12- to 20-fold higher in *Mdr1a/b(−/−)/Bcrp1(−/−)* mice than those in FVBn mice. Likewise, brain-to-plasma ratios were 0.08 in FVBn mice and close to 1 in *Mdr1a/b(−/−)/Bcrp1(−/−)* mice (Table 7). However, the ratio of free brain-to-free plasma concentration was approximately 0.3 (using binding data presented here).

A marked inhibition (~80%) of the PI3K pathway markers pAkt and pS6 was observed in the brains of triple-knockout mice (Fig. 6). Suppression of pS6 was similar at 1 and 6 h, whereas pAkt levels started to recover by 6 h postdose. Inhibition (20–70%) of the pathway also was observed in the brains of wild-type mice, with the suppression of pS6 lasting up to 6 h (Fig. 6).

PK-PD Modeling. *Pharmacokinetic studies.* The parameters (% coefficient of variation) k_a, k_e, and *V*/*F* were estimated for GDC-0980 after single oral administrations to mice of 1, 5, and 10 mg/kg (Fig. 7A) GDC-0980 in MCT and were 0.55 (42) h^{-1}, 0.44 (23) h^{-1}, and 1.18 (32) l/kg, respectively. These estimated parameters were used to simulate plasma concentration-time profiles when modeling the xenograft efficacy data, because serial blood samples adequate for modeling were not collected from tumor-bearing mice during the study. The comparison between observed plasma concentrations and model predictions is presented in Fig. 7B and indicates that the PK model used described these data appropriately.

Xenograft efficacy studies. GDC-0980 was administered orally, daily, to MCF7-neo/HER2 tumor-bearing mice at doses ranging from 0.25 to 7.5 mg/kg. Tumor growth inhibition results are presented in Fig. 7C. The inhibition of the MCF7-neo/HER2 tumor growth appeared to be dose dependent.

An indirect response model was fitted to the tumor data from all of the doses (eq. 1) and appeared to describe them adequately. The comparison between the observed TVs and the model predictions is presented in Fig. 7D. The estimates of the pharmacodynamic parameters describing MCF7-neo/HER2 tumor growth and reduction effect by GDC-0980 are presented in Table 8.

Prediction of Human PK Parameters and Efficacious Doses. Human CL_p and volume of distribution of GDC-0980 were predicted by allometric scaling (Fig. 8) using the estimates of CL_p and volume of distribution from mouse, rat, monkey, and dog. For CL_p, the MLP correction was applied as proposed by Mahmood and Balian (1996), based on the value of the allometric exponent in the simple allometry plot (1; L. Salphati, unpublished observations). The predicted CL_p and volume of distribution were 5.1 ml · min^{-1} · kg^{-1} and 1.8 l/kg, respectively.

The plasma concentration-time profile after oral administration of the starting dose (2 mg) was simulated using GastroPlus. Parameters used as inputs are presented in this article or corresponded to the default values in the software. Plasma CL predicted by allometry was assumed to be equivalent to hepatic CL; thus, hepatic CL was set to 5.1 ml · min^{-1} · kg^{-1} in GastroPlus (21.4 l/h for 70 kg human). The simulated and the average concentrations from patients (Wagner et al., 2009; Bendell et al., 2010) are presented in Fig. 9. The AUC_{0-24}, C_{max}, and $T_{1/2}$ estimated from the GastroPlus simulation (0.13 μM·h, 0.017 μM, and 4.4 h, respectively) are presented in Table 9, along with the actual values obtained in patients in Phase I (Wagner et al., 2009). The fraction absorbed (F_a) and the bioavailability (*F*) predicted by GastroPlus were 99 and 74%, respectively.

The simulated profile was fitted using a one-compartment model with first-order absorption. The estimated parameters from that fit were substituted for the mouse parameters in the PK-PD model described here and used to simulate human doses expected to achieve efficacy. The human daily dose and AUC_{0-24} associated with 60% tumor growth inhibition compared with vehicle on day 21 were 55 mg and 3.8 μM·h, respectively. This dose was determined by iteration,

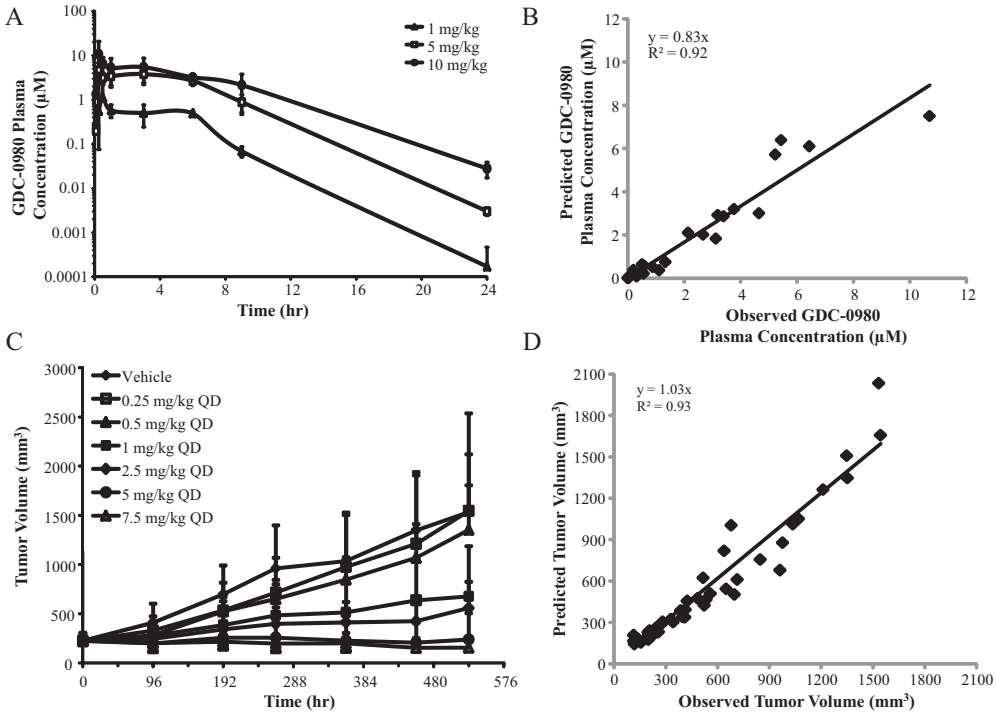

FIG. 7. Plasma concentration-time profiles in nude mice and xenograft studies in MCF7-neo/HER2 tumor-bearing mice. A, concentration-time profiles after oral administration of GDC-0980 at 1, 5, and 10 mg/kg. B, observed versus predicted plasma concentrations obtained by fitting a one-compartment model with first-order absorption. C, TVs versus time after oral administration of GDC-0980 daily at various doses. D, observed versus predicted TVs obtained by fitting of an indirect response model.

TABLE 8

Pharmacodynamic parameters estimated from MCF7-neo/HER2 tumor xenograft studies

Parameter	Estimate	Coefficient of Variation
		%
k_{ng}, h^{-1}	0.0042	2.7
K_{max}, h^{-1}	0.020	11
KC_{50}, μM	2.0	25
n	1 (fixed)	
ED_{60}, mg/kg	1.1	
C_{stasis}, μM	0.52	

through successive simulations of different doses; the target of 60% tumor growth inhibition was reached at 55 mg.

Discussion

The PI3K pathway, which is commonly altered in numerous cancers (Liu et al., 2009a), has been identified as a promising target for the treatment of malignancies. Components of this signaling pathway, such as PI3K or mTOR, can be targeted by small molecules, and several inhibitors specific for one of these two kinases are being evaluated in patients (Engelman, 2009). Inhibitors of mTOR (mTORC1), referred to as rapalogs, have been approved for the treatment of cancers, and numerous dual PI3K/mTOR inhibitors are currently in clinical trials (Benjamin et al., 2011).

Preclinical pharmacokinetic studies provide key parameters during the discovery and the early stages of development of a compound. These parameters help to assess whether sufficient exposure can be achieved in further animal studies (efficacy and toxicology) and also are used to predict pharmacokinetic properties in humans. In addition, when integrated with efficacy data in PK-PD models, they can be used to estimate efficacious and target doses in humans (Gibbs, 2010). GDC-0980, a PI3K/mTOR inhibitor being developed as an anticancer agent, had low plasma CL (and blood CL based on blood-to-plasma ratio) in the mouse, rat, and dog and moderate CL in monkey, compared with hepatic blood flow (Davies and Morris, 1993). Renal CL was a minor route of elimination in monkeys (Table 4), dogs, and rats (Figs. 3 and 4). In contrast, the [^{14}C]GDC-0980-associated radioactivity measured in the bile of BDC rats represented approximately 42% of the dose administered (Fig. 3B), whereas almost all of the dose administered to intact rats was recovered in the feces (Fig. 3A). The combined recovery in urine and bile indicated that 50 to 57% of the oral dose was absorbed. The large contribution of the biliary route in the elimination of GDC-0980 was supported by the results from the rat QWBA study, where high levels of radioactivity were measured in the bile. Likewise, in the dog, biliary elimination was prominent, with >40% of the radioactivity recovered (Fig. 4). Combined with the recovery in urine (21.5%), these results indicated that approximately 63% of the oral dose was absorbed. In both species, the calculated bioavailability (F) was approximately 100%, whereas the fraction absorbed did not appear to exceed 63% based on the recovery of radioactivity in bile and urine. Biliary secretion is a major route of elimination for GDC-0980, and it is possible that it undergoes enterohepatic cycling, after elimination either as the parent compound or as a conjugate cleaved in the intestine, allowing GDC-0980 to be recycled. The reabsorption of the parent compound could contribute to increased AUC and thus F. Indeed, a secondary "hump" can be observed after oral administration in rats and dogs (Fig. 2, A and D), which may be indicative of enterohepatic cycling.

The QWBA study in rats also indicated that GDC-0980 distributed rapidly and extensively into tissues, which was consistent with the moderate volume of distribution measured in the rat PK study. However, among all of the tissues, the levels of radioactivity in the central nervous system were the lowest. This can be attributed to the effect of efflux transporters limiting access of GDC-0980 to the brain. Indeed, despite its high permeability in parental MDCK cells, studies in transfected cells indicated that GDC-0980 was a substrate for P-gp and Bcrp1 (Table 1). These results also were consistent with the poor brain penetration observed in wild-type mice and the marked increase (~20-fold) in brain concentration achieved in the P-gp- and Bcrp1-deficient mice (Table 7). Although the high levels of GDC-0980 in the brains of the knockout mice led to pronounced PI3K pathway suppression, for up to 6 h, inhibition of the pathway was also detected in the brains of wild-type animals (Fig. 6) despite much lower concentrations. The effects observed were consistent with the free brain concentrations determined in both strains (~0.8 μM in the knockout and ~0.06 μM in the wild-type mice), which were greater than the IC_{50} (or K_i) for each of the PI3K isoforms and mTOR (0.005–0.027 μM) (Sutherlin et al., 2011). Similar findings with pAkt were reported with another PI3K inhibitor, 2-(1*H*-indazol-4-yl)-6-(4-methanesulfonyl-piperazin-1-ylmethyl)-4-morpholin-4-yl-thieno[3,2-*d*]pyrimidine (GDC-0941) (Salphati et al., 2010a). However, in addition to this marker, potent inhibition of mTOR by GDC-0980 (Wallin et al., 2011) led to the prolonged suppression of pS6, a downstream effector of mTOR kinase (Fig. 6). Inhibition of PI3K in the brain, through the administration of inhibitors of this pathway in combination with P-gp/BCRP inhibitors or the design of compounds circumventing these transporters, could have implications for the treatment of central nervous system tumors relying on the activation of this pathway, such as glioblastoma (Holand et al., 2011). The fairly constant brain-to-plasma ratio observed between 1 and 6 h suggested that by 1 h a

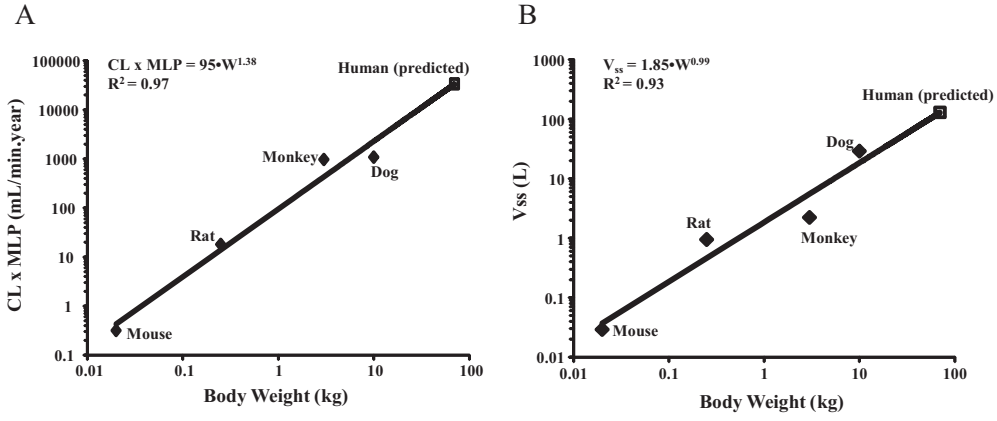

FIG. 8. Predicted human clearance (A) and volume of distribution (B) using allometric scaling.

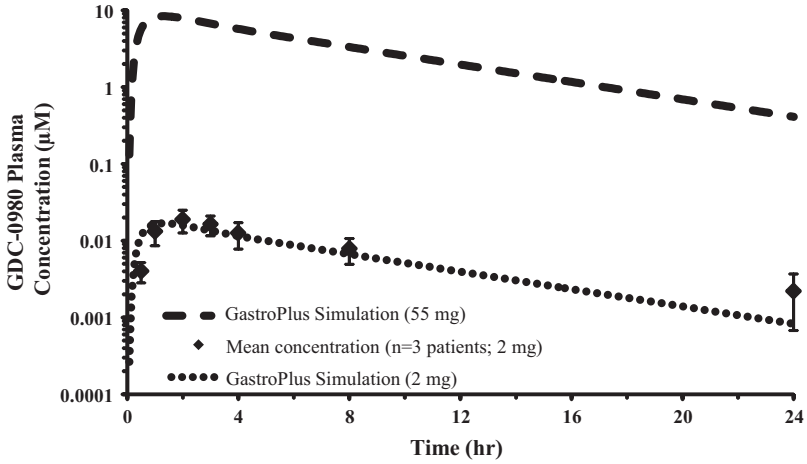

FIG. 9. GastroPlus simulation of plasma concentration-time profile at the starting dose (2 mg) and actual concentrations (±S.D.) measured in patients ($n = 3$) in Phase 1 (Bendell et al., 2010) and simulation at the dose predicted to be associated with 60% tumor growth inhibition.

steady-state condition had been reached between brain and plasma. In addition, the similar plasma concentrations measured in the wild-type and triple-knockout mice implied that the two transporters had minimal impact on systemic exposure to GDC-0980, as has been reported for other substrates of both P-gp and Bcrp1 (Polli et al., 2009; Salphati et al., 2010a). It is worth noting that although GDC-0980 brain penetration was improved markedly in *Mdr1a/b(−/−)/Bcrp1(−/−)* mice, the ratio of free brain-to-free plasma concentrations was approximately 0.3, not approaching 1 as would be expected if free drug was in equilibrium between brain and plasma. Efflux at the blood-brain barrier by transporters other than P-gp and Bcrp1 may explain this result; experimental variability in the estimation of the free fraction in brain or plasma also could contribute to the calculation of this lower than expected free brain-to-plasma ratio. The in vitro determination of binding to brain homogenate nevertheless has been proposed as a reliable method to estimate free brain concentration (Liu et al., 2009b).

Plasma protein binding was low, not exceeding 71% in all of the species over the range of concentrations tested (Table 4), which appeared consistent with the moderate volume of distribution across species (~1–5.6-fold total body water) (Davies and Morris, 1993).

The predicted human CL of GDC-0980 was 5.1 ml · min^{-1} · kg^{-1} using MLP as a correction factor. This predicted human plasma CL was comparable with the hepatic CL of 3.3 ml · min^{-1} · kg^{-1} projected from hepatocyte stability data (Table 2). Plasma CL measured in preclinical species was overall consistent with in vitro projections (Tables 2 and 5), and the narrow range of predictions obtained based on in vitro results and allometry provided some confidence that the human plasma CL would be low. Prediction of human CL remains challenging however, and among the numerous methods evaluated recently (Ring et al., 2011), it did not appear that one was notably more accurate. The use of physiology-based pharmacokinetic models for the prediction of plasma concentration-time oral profiles also resulted in fairly poor performance (Poulin et al., 2011). In general, a thorough characterization and understanding of the preclinical PK, as well as strong in vitro-in vivo correlations in preclinical species, and convergent predictions with different methods provide more confidence. GDC-0980 was generated from the same chemical series as GDC-0941 (Folkes et al., 2008), a compound that had previously entered clinical trials. The evaluation of the different human prediction methods used with that compound (Salphati et al., 2010b) was informative and helped build confidence in the approach selected with GDC-0980. Although the allometry predicted plasma CL and the extrapolation of in vitro hepatocyte stability data predicted hepatic blood CL, these could be compared directly because the blood-to-plasma ratio was 1.1.

The plasma concentration-time profile of GDC-0980 for the starting dose in human (2 mg) was predicted using GastroPlus and the PBPKPlus module. In this simulation, human CL predicted by interspecies scaling (5.1 ml · min^{-1} · kg^{-}) was conservatively chosen as an input for hepatic CL (21.4 l/h; 70 kg human). The PK parameters (AUC, C_{max}, and $T_{1/2}$) derived from the simulation were similar to the values obtained in patients in Phase I (Table 9) (Wagner et al., 2009), and the simulated profile (Fig. 9) described the actual plasma concentrations very closely (Wagner et al., 2009; Bendell et al., 2010). The V_{ss} estimated by PBPKPlus based on the GDC-0980 physicochemical properties and input from in vitro studies also was comparable with that extrapolated from preclinical data by allometry (1.9 versus 1.8 l/kg). To estimate efficacious doses and exposures in human, the parameters obtained from the fit (one-compartment model, first-order absorption) of this simulated profile were substituted for the mouse parameters in the PK-PD model described here. This approach assumes a similar relationship between PD marker response and efficacy in human and mouse xenograft models as well as comparable drug distributions in xenograft and human tumor. Despite these caveats, the prediction of efficacy from PK-PD models of xenograft data can be useful in the design of clinical trials and can help establish PK and PD targets. This method has been applied successfully in predicting targets for human efficacy (Simeoni et al.,

TABLE 9

Predicted (GastroPlus) and observed AUC, C_{max}, and $T_{1/2}$ in human after administration of a 2-mg oral dose and predicted human dose and parameters associated with 60% tumor growth inhibition

Observed data reported as mean ± S.D. ($n = 3$) (Wagner et al., 2009).

Dose	AUC_{0-24}		C_{max}		$T_{1/2}$	
	Predicted	Observed	Predicted	Observed	Predicted	Observed
	μM·h		*μM*		*h*	
2 mg	0.13	0.17 (0.06)	0.017	0.019 (0.005)	4.4	6.4 (2.6)
55 mg	3.8		0.43		4.4	

2004; Tanaka et al., 2008). The GDC-0980 human daily dose and exposure predicted to be associated with 60% tumor growth inhibition were 55 mg and 3.8 μM·h, respectively, based on the MCF7-neo/HER2 xenograft model (PI3K mutant). This target tumor growth inhibition was selected, as proposed by Wong et al. (2011), as the minimum likely to correspond to clinical response. The predicted efficacious dose appeared to be consistent with the results reported by Bendell et al. (2010), showing some clinical response with 50 mg (AUC ~5 μM·h) GDC-0980 dosed daily for 21 days in a 28-day cycle of treatment. Although such consistency is promising, the validity of the preclinical efficacy models also depends on their relevance; the work and predictions presented here were based on the MCF7-neo/HER2 xenograft model (PI3K mutant). Efficacy studies and predictions using models with a different mutational status (e.g., PI3K wild-type, phosphatase and tensin homolog null) also may help to define a range of potential efficacious doses.

In summary, the preclinical absorption, distribution, metabolism, and excretion properties of GDC-0980 provided the basis for further clinical evaluation, and the use of PK and PK-PD simulations in early development helped to assess its potential for clinical efficacy. GDC-0980 is currently in Phase II clinical trials.

Acknowledgments

We thank the Drug Metabolism and Pharmacokinetics, Chemistry, and Small Molecule Pharmaceutical Sciences Departments and the In Vivo Studies Group at Genentech for their contributions to the results presented.

Authorship Contributions

Participated in research design: Salphati, Pang, Plise, Lee, Olivero, Prior, Sampath, and Wong.

Conducted experiments: Plise, Lee, Prior, and Wong.

Contributed new reagents or analytic tools: Zhang.

Performed data analysis: Salphati, Pang, Plise, Lee, and Wong.

Wrote or contributed to the writing of the manuscript: Salphati and Pang.

References

Bendell JC, Wagner AJ, Dolly S, Morgan JA, Papadatos-Pastos D, Ware JA, Mazina KE, Lauchle J, Burris H, and De Bono J (2010) A first-in-human phase I study to evaluate the dual PI3K/mTOR inhibitor GDC-0980 administered QD in patients with advanced solid tumors or non-Hodgkin's lymphoma (NHL). *European Society for Medical Oncology (ESMO) Meeting*; 2010 Oct 8–12, 2010; Milan, Italy. Abstract 4960. ESMO, Viganello-Lugano, Switzerland.

Benjamin D, Colombi M, Moroni C, and Hall MN (2011) Rapamycin passes the torch: a new generation of mTOR inhibitors. *Nat Rev Drug Discov* **10:**868–880.

Boxenbaum H (1982) Interspecies scaling, allometry, physiological time, and the ground plan of pharmacokinetics. *J Pharmacokinet Biopharm* **10:**201–227.

Castanedo G, Dotson J, Goldsmith R, Gunzner J, Heffron T, Mathieu S, Olivero A, Staben S, Sutherlin DP, Tsui V, et al. (2008) Phosphoinositide 3-kinase inhibitor compounds and methods of use. World patent WO/2008/073785. 2008 June 19.

Chalhoub N and Baker SJ (2009) PTEN and the PI3-kinase pathway in cancer. *Annu Rev Pathol* **4:**127–150.

Ciraolo E, Morello F, and Hirsch E (2011) Present and future of PI3K pathway inhibition in cancer: perspectives and limitations. *Curr Med Chem* **18:**2674–2685.

Davies B and Morris T (1993) Physiological parameters in laboratory animals and humans. *Pharm Res* **10:**1093–1095.

Engelman JA (2009) Targeting PI3K signalling in cancer: opportunities, challenges and limitations. *Nat Rev Cancer* **9:**550–562.

Engelman JA, Luo J, and Cantley LC (2006) The evolution of phosphatidylinositol 3-kinases as regulators of growth and metabolism. *Nat Rev Genet* **7:**606–619.

Folkes AJ, Ahmadi K, Alderton WK, Alix S, Baker SJ, Box G, Chuckowree IS, Clarke PA, Depledge P, Eccles SA, et al. (2008) The identification of 2-(1H-indazol-4-yl)-6-(4-methanesulfonyl-piperazin-1-ylmethyl)-4-morpholin-4-yl-thieno[3,2-d]pyrimidine (GDC-0941) as a potent, selective, orally bioavailable inhibitor of class I PI3 kinase for the treatment of cancer. *J Med Chem* **51:**5522–5532.

Gibaldi M and Perrier D (1982) *Pharmacokinetics*, Marcel Dekker, New York.

Gibbs JP (2010) Prediction of exposure-response relationships to support first-in-human study design. *AAPS J* **12:**750–758.

Guertin DA and Sabatini DM (2009) The pharmacology of mTOR inhibition. *Sci Signal* **2:**pe24.

Höland K, Salm F, and Arcaro A (2011) The phosphoinositide 3-kinase signaling pathway as a therapeutic target in grade IV brain tumors. *Curr Cancer Drug Targets* **11:**894–918.

Kalvass JC, Maurer TS, and Pollack GM (2007) Use of plasma and brain unbound fractions to assess the extent of brain distribution of 34 drugs: comparison of unbound concentration ratios to in vivo p-glycoprotein efflux ratios. *Drug Metab Dispos* **35:**660–666.

Liu P, Cheng H, Roberts TM, and Zhao JJ (2009a) Targeting the phosphoinositide 3-kinase pathway in cancer. *Nature Rev Drug Discov* **8:**627–644.

Liu X, Van Natta K, Yeo H, Vilenski O, Weller PE, Worboys PD, and Monshouwer M (2009b) Unbound drug concentration in brain homogenate and cerebral spinal fluid at steady state as a surrogate for unbound concentration in brain interstitial fluid. *Drug Metab Dispos* **37:**787–793.

Mahmood I and Balian JD (1996) Interspecies scaling: predicting clearance of drugs in humans. Three different approaches. *Xenobiotica* **26:**887–895.

O'Reilly KE, Rojo F, She QB, Solit D, Mills GB, Smith D, Lane H, Hofmann F, Hicklin DJ, Ludwig DL, et al. (2006) mTOR inhibition induces upstream receptor tyrosine kinase signaling and activates Akt. *Cancer Res* **66:**1500–1508.

Obach RS, Baxter JG, Liston TE, Silber BM, Jones BC, MacIntyre F, Rance DJ, and Wastall P (1997) The prediction of human pharmacokinetic parameters from preclinical and in vitro metabolism data. *J Pharmacol Exp Ther* **283:**46–58.

Polli JW, Olson KL, Chism JP, John-Williams LS, Yeager RL, Woodard SM, Otto V, Castellino S, and Demby VE (2009) An unexpected synergist role of P-glycoprotein and breast cancer resistance protein on the central nervous system penetration of the tyrosine kinase inhibitor lapatinib (N-{3-chloro-4-[(3-fluorobenzyl)oxy]phenyl}-6-[5-({[2-(methylsulfonyl)ethyl]-amino}methyl)-2-furyl]-4-quinazolinamine; GW572016). *Drug Metab Dispos* **37:**439–442.

Poulin P, Jones RD, Jones HM, Gibson CR, Rowland M, Chien JY, Ring BJ, Adkison KK, Ku MS, He H, et al. (2011) PHRMA CPCDC initiative on predictive models of human pharmacokinetics, part 5: prediction of plasma concentration-time profiles in human by using the physiologically-based pharmacokinetic modeling approach. *J Pharm Sci* **100:**4127–4157.

Ring BJ, Chien JY, Adkison KK, Jones HM, Rowland M, Jones RD, Yates JW, Ku MS, Gibson CR, He H, et al. (2011) PhRMA CPCDC initiative on predictive models of human pharmacokinetics, part 3: comparative assessment of prediction methods of human clearance. *J Pharm Sci* **100:** 4090–4110.

Sabbah DA, Brattain MG, and Zhong H (2011) Dual inhibitors of PI3K/mTOR or mTOR-selective inhibitors: which way shall we go? *Curr Med Chem* **18:**5528–5544.

Salphati L, Lee LB, Pang J, Plise EG, and Zhang X (2010a) Role of P-glycoprotein and breast cancer resistance protein-1 in the brain penetration and brain pharmacodynamic activity of the novel phosphatidylinositol 3-kinase inhibitor GDC-0941. *Drug Metab Dispos* **38:**1422–1426.

Salphati L, Wong H, Belvin M, Bradford D, Edgar KA, Prior WW, Sampath D, and Wallin JJ (2010b) Pharmacokinetic-pharmacodynamic modeling of tumor growth inhibition and biomarker modulation by the novel phosphatidylinositol 3-kinase inhibitor GDC-0941. *Drug Metab Dispos* **38:**1436–1442.

Simeoni M, Magni P, Cammia C, De Nicolao G, Croci V, Pesenti E, Germani M, Poggesi I, and Rocchetti M (2004) Predictive pharmacokinetic-pharmacodynamic modeling of tumor growth kinetics in xenograft models after administration of anticancer agents. *Cancer Res* **64:**1094–1101.

Sutherlin DP, Bao L, Berry M, Castanedo G, Chuckowree I, Dotson J, Folks A, Friedman L, Goldsmith R, Gunzner J, et al. (2011) Discovery of a potent, selective, and orally available class I phosphatidylinositol 3-kinase (PI3K)/mammalian target of rapamycin (mTOR) kinase inhibitor (GDC-0980) for the treatment of cancer. *J Med Chem* **54:**7579–7587.

Tanaka C, O'Reilly T, Kovarik JM, Shand N, Hazell K, Judson I, Raymond E, Zumstein-Mecker S, Stephan C, Boulay A, et al. (2008) Identifying optimal biologic doses of everolimus (RAD001) in patients with cancer based on the modeling of preclinical and clinical pharmacokinetic and pharmacodynamic data. *J Clin Oncol* **26:**1596–1602.

Wagner AJ, Burris HA, De Bono JS, Jayson GC, Bendell JC, Gomez-Roca C, Dolly S, Zee YK, Ware JA, Yan Y, et al. (2009) Pharmacokinetics and pharmacodynamic biomarkers for the dual PI3K/mTOR inhibitor GDC-0980: Initial phase I evaluation. *Mol Cancer Ther* **8 (Suppl 1):**B137.

Wallin JJ, Edgar KA, Guan J, Berry M, Prior WW, Lee L, Lesnick JD, Lewis C, Nonomiya J, Pang J, et al. (2011) GDC-0980 is a novel class I PI3K/mTOR kinase inhibitor with robust activity in cancer models driven by the PI3K pathway. *Mol Cancer Ther* **10:**2426–2436.

Wong H, Choo EF, Alicke B, Ding X, La H, McNamara E, Theil F-P, Tibbitts J, Friedman LS, Hop CECA, et al. (2011) Antitumor activity of targeted and cytotoxic agents in xenograft models correlates with clinical response: A pharmacokinetic-pharmacodynamic analysis. *Mol Cancer Ther* **10 (Suppl 1):**A11.

Wong KK, Engelman JA, and Cantley LC (2010) Targeting the PI3K signaling pathway in cancer. *Curr Opin Genet Dev* **20:**87–90.

Address correspondence to: Dr. Laurent Salphati, Department of Drug Metabolism and Pharmacokinetics, Genentech, Inc., 1 DNA Way, MS 412A, South San Francisco, CA 94080. E-mail: salphati.laurent@gene.com